ARTICLE

Promoting the Stability of Organic Photovoltaics by Planar Heterojunction optimization

Received 00th January 20xx,
Accepted 00th January 20xx

DOI: 10.1039/x0xx00000x

Weixia Lan,[a] Xiaohui Gao,[a] Xian Wu,[a] Qiqi Ding,[a] Wei Shi,[a] Yingjie Liao,[a] Yuanyuan Liu,[a] Wing Chung Tsoi,*[b] and Bin Wei*[a]

In organic photovoltaics (OPV) with bulk heterojunction (BHJ) active layer, the donor and acceptor materials have a metastable nanoscale phase mixture, where the uncontrollable morphology greatly reduces the stability of the device stability. However, OPV with planar heterojunction (PHJ) structures show obvious vertical phase separation, which can provide separately regulated donor and acceptor layers, achieving significantly higher stability when compared to BHJ based devices. In addition, there is relatively little attention paid to understand the internal attenuation mechanism of OPV devices and how to promote its stability for commerical application. In this work, we investigated the stability of OPV devices with both BHJ and PHJ structures, and further discussed the internal mechanisms why PHJ structures could help enhance device stability than BHJ structures. The results showed that after being placed in a nitrogen environment for 240 hours, the power conversion efficiency (PCE) of PBDB-T: ITIC BHJ devices decreased by 92.52%, while the PCE of PBDB-T/ITIC PHJ devices only decreased by 68.79%. When combined with interface reaction and carrier characteristics analyses, it was found that during the aging process of PBDB-T: ITIC BHJ devices, the active layer formed a top surface rich in PBDB-T and a bottom surface rich in ITIC. The adverse interface reaction between PEDOT: PSS hole transport layer and ITIC acceptor accelerated the performance deterioration, while PBDB-T/ITIC PHJ structure can effectively suppress such reaction, resulting in improved device stability. In addition, we also prepared BHJ and PHJ devices with PM6: Y6 system for verification, and the results also demonstrated that PHJ devices exhibited better device stability.

Introduction

Organic photovoltaics (OPVs) offer several distinct advantages, such as low cost, light weight, solution processible, nontoxic, which make it a promising candidate as a renewable energy resource.[1–3] Different methods have been used to improve the performance of OPV devices, such as designing innovative donor and acceptor materials,[4] interface modification,[5] solvent additive,[6,7] and so on. Recently, continuous power conversion efficiency (PCE) improvement has been achieved by utilizing novel donor and acceptor materials.[8,9] However, the main barrier for the commercialization of OPV is the poor device stability. The complex factors disturbing the device stability include oxygen, water, irradiation, heating, metastable morphology[10,11], diffusion of electrodes and buffer layers materials, and mechanical stress.[12] In order to improve the stability of OPV, improvements can be made in material design, structural engineering and encapsulation strategy.

Recently, almost all the remarkable PCE improvements were achieved using the bulk heterojunction (BHJ) structure. In devices with BHJ structure, the donor and acceptor materials blended with each other in nanoscale, and excitons were dissociated within the active layer film via the ubiquitous nanoscale donor/acceptor (D/A) interface; then, the separated electron and hole were transported to the respective electrodes via self-assembled bi-continuous charge channels.[13] However, the formation of BHJ morphology is an extremely complicated process and the formed morphology is also a highly delicate balance involving many parameters such as domain size, purity, miscibility, etc.[14] The optimal BHJ morphology is usually metastable and controlled by thermodynamics, thus resulting in poor device stability.

In order to further accelerate the commercialization of OPV and improve the device stability, sequential donor and acceptor film deposition is proposed to form planar heterojunction (PHJ), which is attractive in the regard that the morphology of D/A components can be controlled more independently.[15] The extraction of photogenerated carriers toward the two electrodes can be facilitated with more stable vertical phase separation,[16] which is conducive to maintaining the device stability. In addition, the interpenetration between donor and acceptor during the solution processing ensures the clear D/A interfaces for charge separation.[17] The bilayer structure in PHJ should be more favourable for charge transport as the separated charges can be easily transported to the corresponding electrode through the donor or acceptor layer with low recombination possibility.[18] As both donor and acceptor layers can be processed and optimized independently, this PHJ is less dependence on the D/A ratio, solvent and additive. Therefore, the morphology and device design of PHJ devices can be better controlled to achieve improved device stability. However, in comparison with BHJ OPV, there are only a few papers reported on

[a] School of Mechatronic Engineering and Automation, Shanghai University, Shanghai, 200444, China
[b] SPECIFIC, College of Engineering, Swansea University, Swansea, United Kingdom
E-mail: w.c.tsoi@swansea.ac.uk; bwei@shu.edu.cn

the stability investigation of the sequentially deposited PHJ structure devices.

In this work, we focused on the internal mechanism of PHJ structure during the device aging in nitrogen environment, and made careful comparison with BHJ structure. Devices with both PBDB-T: ITIC and PM6: Y6 systems are designed and evaluated. Our results expressly announced that the stability of all PHJ devices is significantly higher than that of BHJ devices, which shows that PHJ structure has obvious advantages over BHJ structure in improving the device stability, proving novel strategy for improving the device stability of OPVs.

Results and discussion

Analysis of Thin Film Interface Reaction

Firstly, the interface reaction analysis based on PBDB-T: ITIC BHJ film and PBDB-T/ITIC PHJ film is conducted. With the absorption spectra show in Fig. 1.

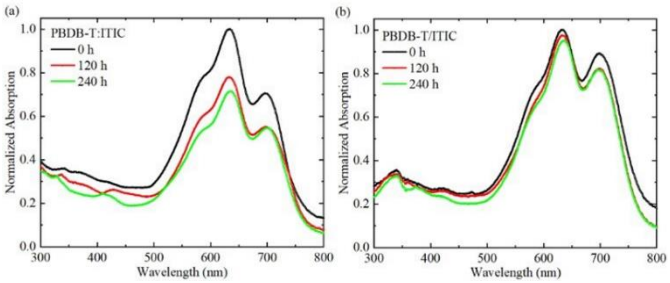

Fig. 1 Absorption spectra at different time periods: (a) PEDOT: PSS/PBDB-T: ITIC thin film, (b) PEDOT: PSS/PBDB-T/ITIC thin film.

From Fig. 1, it can be seen that after being placed in a nitrogen environment for 240 h, the absorption intensity of the BHJ film significantly decreases, while the absorption intensity of the PHJ film only undergoes a slightly decreases. The rapid decrease in absorption intensity indicates a sharp decrease in exciton generation efficiency, while maintaining stable light absorption efficiency is a prerequisite for excellent OPV operation. The absorption results have shown that PHJ structures are superior to BHJ structures in maintaining the exciton generation stability.

Fig. S1 is an Atomic Force Microscope (AFM) diagram result based on PBDB-T: ITIC BHJ and PBDB-T/ITIC PHJ films at 0 and 120 hours, where the bright and dark domains in the figure correspond to PBDB-T and ITIC, respectively.

From Fig. S1, it can be seen that at 0 hours, the PHJ film has more dark domains compared to the BHJ film, indicating that the top of the PHJ film is enriched with more ITIC, which can effectively suppress the adverse interface reaction between PEDOT: PSS and ITIC, and help improve device stability. However, in BHJ films, the interface reaction between PEDOT: PSS and ITIC cannot be avoided. Our previous results have proved that the adverse interface reaction between PEDOT: PSS and ITIC can accelerate the aging of the device, resulting in poor device stability. In addition, for PHJ structures, according to the principle of entropy increase, the donor and acceptor materials will spontaneously diffuse with each other, which will help increase the D/A interface in the PHJ structure and compensate for the defect of insufficient D/A interface.[19-21] From the 120 hour AFM graph, it can be seen that the bright region of the PHJ film increases, and the proportion of D/A interfaces is improved.

Table S1 lists the roughness values of BHJ and PHJ films measured by AFM. It can be seen that compared to PBDB-T: ITIC BHJ films, the surface of PBDB-T/ITIC PHJ films is more uniform. At 0 hours, the surface roughness of the PBDB-T: ITIC BHJ film is 2.84 nm, while it is 1.47 nm for the PBDB-T/ITIC PHJ film; At 120 hours, the surface roughness of the PBDB-T: ITIC BHJ film was increased to 6.10 nm, while it was almost unchanged for the PHJ film. From the RMS roughness values at different time periods, it can be seen that the surface roughness of BHJ films changes significantly, and an increase in roughness is not conducive to the transmission and collection of charges. However, the surface roughness of PHJ films remains basically unchanged, indicating that the surface composition of PHJ films is more stable and uniform, which is conducive to the charge extraction.

In addition, it has been reported that the vertical layering of BHJ and PHJ films is related to the surface energy shift of D/A materials.[22-24] Frequently used acceptor materials with high surface energy tend to spontaneously aggregate on substrates with high surface energy, such as PEDOT: PSS substrates. Therefore, further research was conducted on the surface energy analysis of different heterojunction films to verify the surface composition of BHJ and PHJ film.

The contact angle of water on neat PBDB-T and ITIC films are measured to be 116.3°and 105.5°, respectively, which are almost unchanged after 120 h. The surface energy values are calculated to be 21.54 and 27.19 mN/m for neat PBDB-T and ITIC films, respectively. The test results of water contact angle and ethylene glycol contact angle based on PBDB-T: ITIC BHJ film and PBDB-T/ITIC PHJ film at different time periods are shown in Fig. S2. Table 1 summarizes the values of contact angle.

Table 1 Contact angle test values based on PEDOT: PSS/PBDB-T: ITIC film and PEDOT: PPS/PBDB-T/ITIC film.

Device	Time	Contact angle	
		deionized water	ethylene glycol
PBDB-T: ITIC	0 h	89.96°	70.00°
	24 h	91.52°	69.06°
	120 h	84.86°	59.06°
PBDB-T/ITIC	0 h	91.51°	68.47°
	24 h	91.76°	69.61°
	120 h	87.02°	63.19°

The surface energy of the thin film was calculated using the Owens method. According to formulas 1 and 2, the surface energy parameters and component values of PBDB-T: ITIC BHJ thin film and PBDB-T/ITIC PHJ thin film can be calculated respectively.

$$1 + \cos\theta = 2 \times \left(\sqrt{\gamma^d} \times \frac{\sqrt{\gamma_L{}^d}}{\gamma_L} + \sqrt{\gamma^p} \times \frac{\sqrt{\gamma_L{}^p}}{\gamma_L} \right) \quad (1)$$

$$\gamma = \gamma^d + \gamma^p \quad (2)$$

The known value in the equation is the contact angle value θ, dispersion component of solvent $\gamma_L{}^d$, polarity component $\gamma_L{}^p$, what needs to be calculated is the dispersion component, polarity component, and surface energy of the material. The dispersion and polarity components of deionized water and ethylene glycol used to calculate the surface energy of the thin films are summarised in Table S2. The surface energy values are calculated in Table 2. It can be seen

that at 0 hours, the surface energy based on PBDB-T/ITIC film is higher than that of PBDB-T: ITIC film, indicating that in the PBDB-T/ITIC structure, ITIC mainly aggregates at the top of the film, which can effectively avoid adverse interface reactions between ITIC and PEDOT: PSS. However, for the PBDB-T: ITIC structure, it cannot avoid interface reactions between ITIC and PEDOT: PSS. After 24 hours, the surface energy of PBDB-T/ITIC film decreased, indicating that more D/A interfaces were formed in the PHJ film , which was beneficial for maintaining the stability of the device.

Table 2 Surface energy based on PEDOT: PSS/PBDB-T: ITIC thin films and PEDOT: PPS/PBDB-T/ITIC thin films.

Device	Time	Parameters（mN/m）		
		γ^d	γ^p	γ
PBDB-T: ITIC	0 h	16.56	5.63	22.19
	24 h	21.17	3.23	24.40
	120 h	24.33	5.08	29.41
PBDB-T/ITIC	0 h	20.63	3.70	24.33
	24 h	19.37	3.98	23.35
	120 h	21.71	5.03	26.74

Note: γ^d is the dispersion component, γ^p is the polarity component.

Analysis of Photovoltaic Performance of Devices

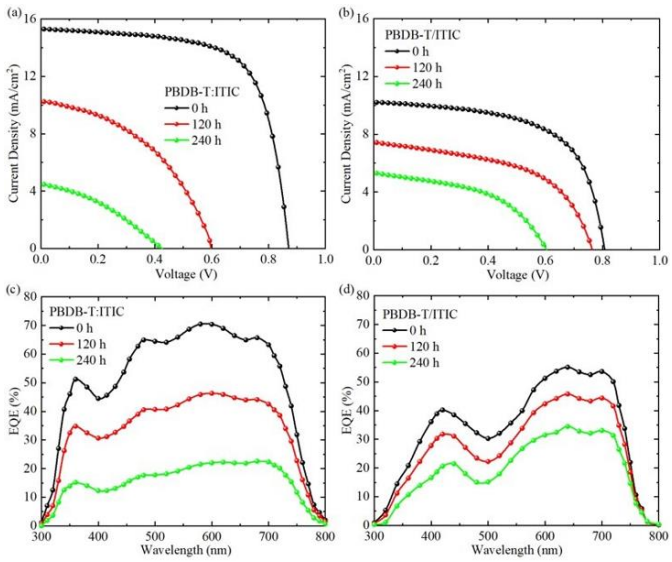

Fig. 2 Based on PBDB-T: ITIC BHJ and PBDB-T/ITIC PHJ OPV: (a) (b) J-V curves at different time periods, (c) (d) EQE curves at different time periods.

For devices with PBDB-T: ITIC BHJ and PBDB-T/ITIC PHJ structure, the current density-voltage (*J-V*) curves and external quantum efficiency (EQE) curves at different time periods are shown in Fig. 2. It can be seen that the *J-V* curve and EQE curve of the PHJ device showed a much lower decrease compared to the BHJ device, proving that the PHJ device has more stable photoelectric conversion ability. In addition, after 240 hours, the PCE of PBDB-T:ITIC BHJ devices by 92.52%, while the PCE of PBDB-T/ITIC PHJ devices only decreased by 68.79%, indicating that the PHJ-based OPV has better stability performance.

Fig. 3 summarized the PCE histograms of BHJ and PHJ OPVs (when PCE drops to 30%). It can be seen that when PCE of PBDB-T: ITIC BHJ devices and PBDB-T/ITIC PHJ devices drops to 30% of the initial value, the number of devices conforms to the normal distribution, indicating the reliability of the results. The PCE of PBDB-T: ITIC BHJ devices decreases to 30% of the initial PCE after 120 hours, while the PCE of PBDB-T/ITIC PHJ devices decreases to 30% of the initial PCE after 250 hours. This result further indicates that the PHJ OPV has good stability and repeatability.

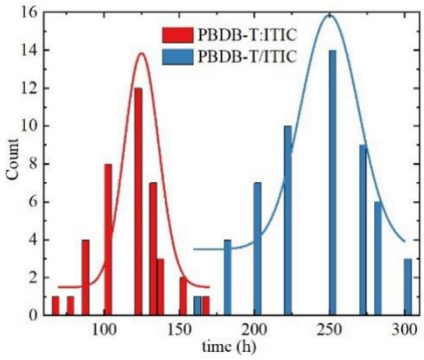

Fig. 3 PCE histograms of BHJ and PHJ OSCs (when PCE drops to 30%).

Analysis of Device Carrier Characteristics

To analysis the carrier characteristics of different devices. Fig. 4 shows a comparison of the charge collection efficiency (η_{CC}) between BHJ and PHJ devices at different time periods. η_{CC} is a function of light intensity (I) and effective voltage (V_{eff}), which can be analysed using formulas (3):

$$\eta_{CC}(I, V_{eff}) = \frac{J_{ph}(I,V_{eff})}{J_{ph,\ sat}(I,V_{eff})} \quad (3)$$

where I represents light intensity, $J_{ph} = J_l - J_d$, J_{ph} represents the current density measured under light, J_d represents the dark current density. The effective voltage $V_{eff} = V_0 - V_a$, where V_0 is the built-in voltage, V_a is the applied voltage. $J_{ph,\ sat}$ is the saturated photocurrent density, J_{ph} decreases faster at low V_{eff}, indicating more severe composite losses in this stage. Fig. 4 show the η_{CC} comparison of PBDB-T: ITIC BHJ devices and PBDB-T/ITIC PHJ devices at different time periods, It can be seen that the η_{CC} of BHJ devices decreases much faster than that of PHJ devices. After 240 hours, for BHJ devices operating at Maximum Power Point (P_{max})(V_{eff} around 0.20 V), a decrease of 47.56% was observed, while in PHJ devices, a decrease of only 27.89% was observed, indicating that PHJ devices exhibited more stable charge extraction properties than BHJ devices, which is a important condition for excellent device stability.

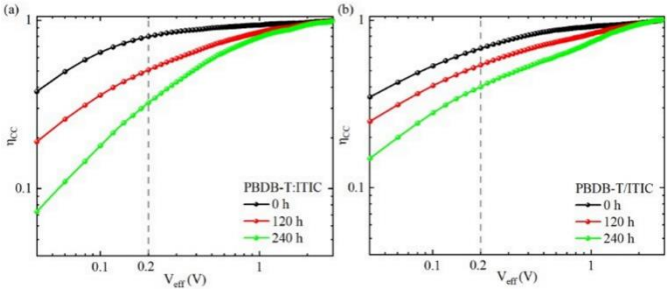

Fig. 4 Normalized η_{CC} as a function of V_{eff}: (a) PBDB-T: ITIC BHJ OPV, (b) PBDB-T/ITIC PHJ OPV.

In addition, hole mobility is closely related to charge extraction performance.[25] Hole-only devices have been fabricated with structure of ITO/PEDOT:PSS/PBDB-T:ITIC/MoO3/Al、ITO/PEDOT: PSS /PBDB-T/ITIC/MoO3/Al. Fig. S3 shows the $J^{0.5} - V$ characteristics of different devices calculated using the Space Charge Limited Current (SCLC) method. The specific value of hole mobility can be obtained by using Mott Gunney's law,[26] which can be expressed with formula (4):

$$J = \frac{9}{8}\varepsilon_r \varepsilon_0 \mu \frac{V^2}{L^3} \quad (4)$$

where J is the space charge limit current density; ε_r and ε_0 are the vacuum dielectric constant and relative dielectric constant of the photosensitive material; V is the applied bias voltage; L is the thickness of the active layer; μ represents the carrier mobility.

From Fig. S3, it can be seen that after 240 hours, the hole mobility of PBDB-T: ITIC BHJ devices decreased from 1.76×10^{-4} $cm^2V^{-1}s^{-1}$ to 0.13×10^{-4} $cm^2V^{-1}s^{-1}$, with the migration rate decreased by 92.61%, while the migration rate based on PBDB-T/ITIC PHJ devices decreased from 0.97×10^{-4} $cm^2V^{-1}s^{-1}$ to 0.32×10^{-4} $cm^2V^{-1}s^{-1}$, which only decreased by 67.01%. At 0 hours, the mobility of PHJ devices is lower than that of BHJ devices, indicating that the charge extraction performance of BHJ devices is better. However, after 240 hours, the mobility of PHJ devices is significantly higher than that of BHJ devices. This indicates that the adverse interface reaction between PEDOT: PSS transport layer and ITIC acceptor in the BHJ structure can significantly reduce the charge extraction performance of the device, The PHJ structure effectively suppresses the interface reaction between PEDOT: PSS and ITIC, which is conducive to maintaining good charge extraction performance and improving the stability of the PHJ device.

Fig. 5 shows the schematic diagram of the exciton behaviour based on different heterojunction structures at initial stage (0 hours). From Figure 5, it can be seen that at the initial stage, the BHJ structure exhibits stronger light absorption ability, which will generate more excitons. At the same time, due to the nanoscale phase mixing of the BHJ structure, it promotes better exciton dissociation and charge transfer at the initial stage. However, the BHJ structure also suffer severe interface reaction between PEDOT: PSS and nnfullerence acceptor, reducing the light absorption ability of the thin film, thereby accelerating the aging of the BHJ device. However, the significant vertical phase separation in PHJ structure shortens the charge transfer path and suppresses charge recombination, which is beneficial for maintaining device stability.

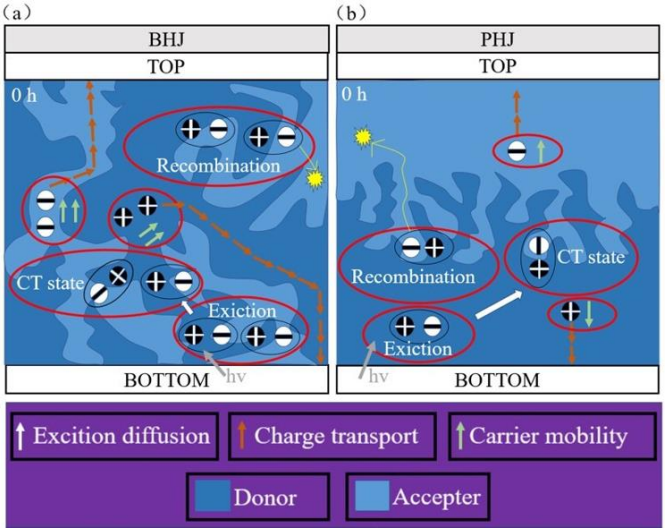

Fig. 5 Schematic diagram of exciton and charge carrier behaviour at 0 hours: (a) BHJ structure, (b) PHJ structure.

Fig. 6 shows the schematic diagram of exciton and carrier behaviour based on PBDB-T: ITIC BHJ structure and PBDB-T/ITIC PHJ structure at 120 hours. From Figure 6, it can be seen that after 120 hours of storage, due to the adverse interface reaction between PEDOT: PSS and ITIC, the light absorption capacity of the BHJ film was significantly reduced, resulting in a sharp decrease of excitons generation. However, the PHJ structure maintained a more stable exciton production efficiency. The film quality of the BHJ structure was deteriorated, which was less conducive to charge transfer, causing a sharp decrease in carrier mobility and device efficiency. The PHJ structure, on the other hand, still has good film quality, enabling the device to obtain stable charge extraction ability and good device stability. At the same time, the PHJ structure increases the D/A interface due to mutual diffusion between donor and acceptor materials. Thus, when compared to the BHJ structure, the PHJ structure could help to improve device stability.

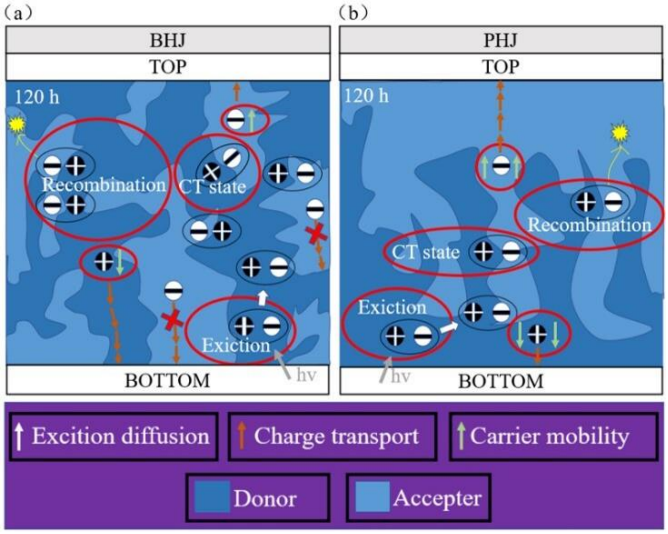

Fig. 6 Schematic diagram of exciton and charge carrier behaviour at 120 hours: (a) BHJ structure, (b) PHJ structure.

Moreover, the initial nanoscale phase separation of the donor and acceptor in the BHJ structure provide the ideal interpenetrating

network morphology. However, it could also increase partial optical loss of the devices by light scattering and the parasite absorption caused by a large number of D/A interfaces in the BHJ active layer.[27] On the contrary, the PHJ structure has relatively less D/A interface, facilitating the reduction of light scattering and parasite absorption. The more obvious vertical phase separation in the PHJ structure is beneficial for better charge transfer.[28]

Device stability results

The unpackaged devices were stored in a glove box filled with nitrogen gas during the aging test. Fig. 7 shows the relationship between normalized PCE, J_{SC}, *FF* and V_{OC} and aging time for PBDB-T: ITIC BHJ devices and PBDB-T/ITIC PHJ devices. It can be seen that the device based on PBDB-T/ITIC PHJ has better nitrogen stability. After 240 hours, the J_{SC} of devices based on PBDB-T: ITIC BHJ decreased by 70.46%, V_{OC} decreased by 52.87%, *FF* decreased by 47.60%, and PCE decreased by 92.52%. In contrast, the J_{SC} of devices based on PBDB-T/ITIC PHJ only decreased by 47.70%, V_{OC} decreased by 24.69%, *FF* decreased by 20.97%, and PCE decreased by 68.79%. The device performance data for different time periods are summarized in Table S3.

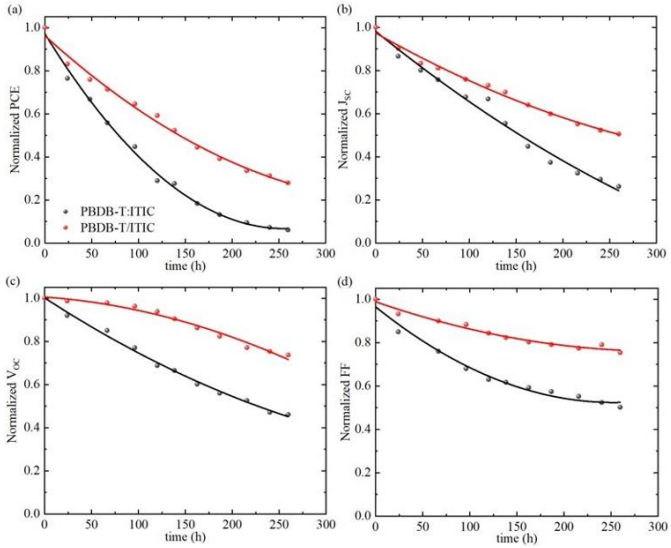

Fig. 7 Normalized (a) PCE, (b) J_{SC}, (c) V_{OC}, and (d) FF as a function of the aging time for devices based on PBDB-T: ITIC BHJ and PBDB-T/ITIC PHJ.

The changes in R_S values in Table S3 can also reflect the changes in device stability. Compared to BHJ devices, PHJ devices exhibit smaller R_S changes after 240 hours, indicating that the degree of internal current loss in the device is smaller, which helps to improve device stability.

Aging time dependent $J-V$ characteristics of PM6:Y6-based OPVs are also explored with different heterojunction structures. The corresponding aging time dependent performance is summarized in fig. S4. The results indicate that PHJ devices based on PM6/Y6 structure have better stability. After placing the BHJ device based on PM6: Y6 for 24 hours, it was observed that the J_{SC} was 71.00% of the initial value, V_{OC} is 59.52% of the initial value, *FF* is 71.07% of the initial value and PCE is 30.03% of the initial value. In contrast, under the same conditions, the stability of PHJ devices based on PM6/Y6 structure is better, with J_{SC} being 82.23% of the initial value, V_{OC} is 75.90% of the initial value, *FF* is 78.09% of the initial value and PCE is 48.72% of the initial value. The device performance data for different time periods are summarized in Table S4.

Experimental

Fig. S5 is a schematic diagram of the device structure designed in this work.

The specific device structure is:

Device 1：ITO/PEDOT:PSS/PBDB-T:ITIC/BCP/Al

Device 2：ITO/PEDOT:PSS/PBDB-T/ITIC/BCP/Al

Device 3：ITO/PEDOT:PSS/PM6:Y6/BCP/Al

Device 4：ITO/PEDOT:PSS/PM6/Y6/BCP/Al

Fig. S6 is the active layer material used in this work, fig. S6 (a) is the donor material PBDB-T, fig. S6 (b) is the acceptor material ITIC, fig. S6 (c) is the donor material PM6, and fig. S6 (d) is the receptor material Y6.

Fig. S7 is a flowchart of the different active layer structures prepared in this work, where fig. S7 (a) is the flowchart of preparing PHJ structures and fig. S7 (b) is the flowchart of preparing BHJ structures.

The specific preparation process of the device is:

Patterned ITO electrode was cleaned by sequential sonication in acetone, soap, deionized water, and isopropanol. In the BHJ devices, the polymer PBDB-T: ITIC mixture (D: A = 1:1, Solarmer Materials Inc) was dissolved in chlorobenzene (CB) for 20 mg/ml and stirred at room temperature overnight. The PM6:Y6 (D: A = 1:1.2, Solarmer Materials Inc) mixture was dissolved in chloroform (CF) for 15.8 mg/ml. In the PHJ devices, PBDB-T were dissolved in CB for 10 mg/ml. ITIC was dissolved in OX for 8 mg/ml. PM6 were dissolved in CF for 8 mg/ml. ITIC was dissolved in CF for 8 mg/ml. The specific process of device preparation is as follows, PEDOT: PSS (CLEVIOS P VP AI 4083) was subsequently prepared on ITO (3000 rpm, 1 min), the PBDB-T:ITIC layer was spin-coated at 2000 or 2250 rpm for BHJ devices. In the PHJ devices, the PBDB-T layer was spin-coated with different revolutions (from 1000 to 3000rpm), and an upper ITIC layer was spin-coated with different revolutions (from 1000 to 3000 rpm) after a 20 min delay for PHJ devices. Finally, 8 nm BCP electron extraction layer and 120 nm thick Al upper contact were deposited on the BHJ and PHJ by the thermal evaporation. The effective area of the devices is 0.04 cm2. The J–V characteristics of the OSCs were measured using a calibrated AM 1.5G solar simulator (ABET Sun2000). EQE spectra of the OSCs were measured using a 7-SCSpec solar cell measurement system (7-STAR Co.).

Contact angle measurements of the films were performed at a Krüss DSA100s Drop Shape Analyzer. Water (72.8 mN m−1, 25°C) and glycol were used as probe liquids.

The surface morphology of the films was analyzed using AFM (Nanonavi SPA-400SPM) measurements.

The absorption spectra of the films were measured using a UV–vis spectrophotometer (HITACHI Ue3900H).

Conclusions

In summary, we have developed high stability OPV based on PBDB-T/ITIC PHJ using a sequentially deposited bilayer structure. A

PBDB-T-rich top surface and an ITIC-rich bottom surface in PBDB-T: ITIC BHJ were observed during the aging period. The poor stability of BHJ, caused by the unavoidable interfacial reaction between PEDOT: PSS and ITIC, is responsible for the deterioration in the long-term operational stability of the PBDB-T: ITIC OPV. The use of PHJ structure benefits the efficient operation of OPV through suppression of interfacial reaction between the PEDOT: PSS and the ITIC. The excellent performance of the bilayer structure device can be ascribed to the graded donor and acceptor distribution during the solution processing, which is believed to be an ideal structure for OPV. Moreover, as the acceptor is hidden behind the polymer donor, the possibility of PEDOT: PSS reacting with ITIC is reduced. Thus, improved stability was observed in the PHJ structure device when compared with the BHJ device. Besides, in PM6:Y6 system, the stability of PHJ structure is also better than that of BHJ structure, it shows that PHJ structure is universal in improving the stability of devices. So far, there are few reports on the stability of PHJ structure. The findings of this work will help us to improve the understanding with novel device design knowledge for developing high-efficiency and stable OPV.

Author Contributions

W. Lan conducted experiments and drafted the manuscript. X. Gao fabricated devices and tested device performance. X. Wu conducted aging test of the devices. Q. Ding carried out the absorption spectra measurements and data analysis. W. Shi carried out the AFM measurements and data analysis. Y. Liao carried out the contact angle measurements and data analysis. Y. Liu participated provided result analysis and drawings. W. Tsoi contributed to reviewing and editing the article. B. Wei contributed to overall project management and reviewing and editing the article.

Conflicts of interest

There are no conflicts to declare.

Acknowledgements

This work was financially supported by the National Natural Science Foundation of China (62005152, 61973206).

References

1 K. Jin, Z. Xiao and L. Ding, 18.69% PCE from organic solar cells. *Journal of Semiconductors*, 2021, **42**, 060502.
2 Q. Wu, W. Wang, Y. Wu, Z. Chen, J. Guo, R. Sun, J. Guo, Y. Yang and J. Min, High-Performance All-Polymer Solar Cells with a PseudoBilayer Configuration Enabled by a Stepwise Optimization Strategy, *Advanced Functional Materials*, 2021, **31**, 2010411
3 W. Lan, J. Gu, X. Gao, Ch. Gong, Y. Liu, W. Zhang, Y. Sun, T. Yue, B. Wei and Furong Zhu，Efficient and Ultraviolet-durable Nonfullerene Organic Solar Cells: from Interfacial Passivation and Microstructural Modification Perspectives, *Advanced Materials Interfaces*, 2022, 9, 2101894.
4 V. Vohra, N. T. Razali, R. Wahi, L. Ganzer and T. Virgili, A Comparative Study of Low-Cost Coating Processes for Green & Sustainable Organic Solar Cell Active Layer Manufacturing, *Optical Materials: X*, 2022, **13**, 100127.
5 J. J. Shen, Recently-Explored Top Electrode Materials for Transparent Organic Solar Cells, *Synthetic Metals*, 2021, **271**, 116582.
6 W. H. Peng, Y. B. Lin, S. Y. Jeong, Z. Genene, A. Magomedov, H. Y. Woo, C. L. Chen, W. Wahyudi, Q. Tao, J. Y. Deng, Y. Han, V. Getautis, W. G. Zhu, T. D. Anthopoulos and E. G. Wang, Over 18% Ternary Polymer Solar Cells Enabled by a Terpolymer as the Third Component, *Nano Energy*, 2022, **92**, 106681.
7 F. W. Zhao, H. T. Zhang, R. Zhang, J. Yuan, D. He, Y. P. Zou and F. Gao, Emerging Approaches in Enhancing the Efficiency and Stability in Non-Fullerene Organic Solar Cells, *Advanced Energy Materials*, 2020, **10**, 2002746.
8 L. P. Duan, N. K. Elumalai, Y. Zhang and A. Uddin, Progress in Non-Fullerene Acceptor Based Organic Solar Cells, *Solar Energy Materials and Solar Cells*, 2019, **193**, 22-65.
9 J. Munshi, U. F. Ghumman, A. Iyer, R. Dulal, W. Chen, T. Y. Chien and G. Balasubramanian, Effect of Polydispersity on the Bulk-Heterojunction Morphology of P3HT:PCBM Solar Cells, *Journal of Polymer Science Part B- Polymer Physics*, 2019, **57**, 895-903.
10 Q. He, W. Sheng, M. Zhang, G. Xu, P. Zhu, H. Zhang, Z. Yao, F. Gao, F. Liu, X. Liao and Y. Chen, Revealing Morphology Evolution in Highly Efficient Bulk Heterojunction and Pseudo-Planar Heterojunction Solar Cells by Additives Treatment, *Advanced Energy Materials*, 2021, **11**, 2003390.
11 W. Lan, J. Gu, S. Wu, Y. Peng, M. Zhao, Y. Liao, T. Xu, B. Wei, L. Ding, F. Zhu, Toward improved stability of nonfullerene organic solar cells: Impact of interlayer and built-in potential, *EcoMat*, 2021, **3**, e12134.
12 P. R. Berger and M. Kim, Polymer Solar Cells: P3ht:Pcbm and Beyond, J*ournal of Renewable and Sustainable Energy*, 2018, **10**, 013508.
13 G. Y. Zhang, J. B. Zhao, P. C. Y. Chow, K. Jiang, J. Q. Zhang, Z. L. Zhu, J. Zhang, F. Huang and H. Yan, Nonfullerene Acceptor Molecules for Bulk Heterojunction Organic Solar Cells, *Chemical Reviews*, 2018, **118**, 3447-3507.
14 S. H. Park, A. Roy, S. Beaupre, S. Cho, N. Coates, J. S. Moon, D. Moses, M. Leclerc, K. Lee and A. J. Heeger, Bulk Heterojunction Solar Cells with Internal Quantum Efficiency Approaching 100%, *Nature Photonics*, 2009, **3**, 297-302.
15 D. F. Zhang, W. K. Zhong, L. Ying, B. B. Fan, M. J. Li, Z. Q. Gan, Z. M. Zeng, D. C. Chen, N. Li, F. Huang and Y. Cao, Overcoming Incompatibility of Donors and Acceptors by Constructing Planar Heterojunction Organic Solar Cells, *Nano Energy*, 2021, **85**, 105957.
16 L. Q. Huang, P. Jiang, Y. D. Zhang, L. F. Zhang, Z. K. N. Yu, Q. N. He, W. H. Zhou, L. C. Tan and Y. W. Chen, Unraveling the Morphology in Solution-Processed Pseudo-Bilayer Planar Heterojunction Organic Solar Cells, *ACS Applied Materials & Interfaces*, 2019, **11**, 26213-26221.
17 Y. Liu, F. Liu, H. W. Wang, D. Nordlund, Z. W. Sun, S. Ferdous, T. P. Russell, Sequential Deposition:Optimization of Solvent Swelling for High-Performance Polymer Solar Cells, *ACS Applied Materials Interfaces*, 2015, **7**, 653-661.
18 A. J. Clulow, C. Tao, K. H. Lee, M. Velusamy, J. A. McEwan, P. E. Shaw, N. L. Yamada, M. James, P. L. Burn, I. R. Gentle and P. Meredith, Time-Resolved Neutron Reflectometry and Photovoltaic Device Studies on Sequentially Deposited PCDBTBT-Fullerene Layers, *Langmuir*, 2014, **30**, 11474-11484.
19 M. Zeng, X. J. Wang, R. J. Ma, W. Y. Zhu, Y. Li, Z. X. Chen, J. W. Zhou, W. Q. Li, T. Liu, Z. C. He, H. Yan, F. Huang and Y. Cao, Dopamine Semiquinone Radical Doped Pedot:Pss: Enhanced Conductivity, Work Function and Performance in

Organic Solar Cells, *Advanced Energy Materials*, 2020, **10**, 2000743.
20 J. Hwang, F. Amy and A. Kahn, Spectroscopic Study on Sputtered Pedot·Pss: Role of Surface Pss Layer, *Organic Electronics*, 2006, **7**, 387-396.
21 J. Bertrandie, A. Sharma, N. Gasparini, D. R. Villalva, S. H. K. Paleti, N. Wehbe, J. Troughton and D. Baran, Air-Processable and Thermally Stable Hole Transport Layer for Non-Fullerene Organic Solar Cells, *ACS Applied Energy Materials*, 2022, **5**, 1023-1030.
22 A. C. Arias, J. D. Mackenzie, R. Stevenson, J. J. M. Halls, M. Inbasekaran, E. P. Woo, D. Richards and R. H. Friend, Photovoltaic Performance and Morphology of Polyfluorene Blends: A Combined Microscopic and Photovoltaic Investigation, *Macromolecules*, 2001, **34**, 6005-6013.
23 H. Yan, Z. H. Chen, Y. Zheng, C. Newman, J. R. Quinn, F. Dotz, M. Kastler and A. Facchetti, A High-Mobility Electron-Transporting Polymer for Printed Transistors, *Nature*, 2009, **457**, 679-686.
24 M. Schubert, D. Dolfen, J. Frisch, S. Roland, R. Steyrleuthner, B. Stiller, Z. H. Chen, U. Scherf, N. Koch, A. Facchetti and D. Neher, Influence of Aggregation on the Performance of All-Polymer Solar Cells Containing Low-Bandgap Naphthalenediimide Copolymers, *Advanced Energy Materials*, 2012, **2**, 369-380.
25 S. A. Jenekhe and S. J. Yi, Efficient Photovoltaic Cells from Semiconducting Polymer Heterojunctions, *Applied Physics Letters*, 2000, **77**, 2635-2637.
26 Q. Liao, Q. Kang, Y. Yang, Z. Zheng, J. Z. Qin, B. W. Xu and J. H. Hou, Highly Stable Organic Solar Cells Based on an Ultraviolet-Resistant Cathode Interfacial Layer, *CCS Chemistry*, 2022, **4**, 938-948.
27 S. Liu, H. Li, X. Wu, D. Chen, L. Zhang, X. Meng, L. Tan, X. Hu and Y. Chen, Pseudo-Planar Heterojunction Organic Photovoltaics with Optimized Light Utilization for Printable Solar Windows, *Advanced Materials*, 2022, **34**, 2201604.
28 Q. He, W. Sheng, M. Zhang, G. Xu, P. Zhu, H. Zhang, Zh. Yao, F. Gao, F. Liu, X. Liao, and Y. Chen, Revealing Morphology Evolution in Highly Efficient Bulk Heterojunction and Pseudo-Planar Heterojunction Solar Cells by Additives Treatment, *Advanced Energy Materials*, 2021, **11**, 2003390.